590672

Occurrence and Forms of Water and Ice on the Earth and Beyond, and the origin(s) of life

David Blake
NASA Ames Research Center
Moffett Field, CA 94035

ABSTRACT

The natural history of the biogenic elements (H,C,O,N) from their first association within cold molecular clouds to their delivery to the Earth during the late bombardment of the inner solar system, is intimately linked to water ice. The earliest organic compounds are formed in cold interstellar molecular clouds as a result of UV and thermal processing of sub-μm ice grains which contain trapped carbon and nitrogen molecules. Structural changes in the water ice host underlie and fundamentally control important macroscopic phenomena such as the outgassing of volatiles, the rates of chemical reactions, and processing and retention of organic compounds. Prebiotic organic material was in all likelihood delivered the early Earth in a pristine state as a consequence of its sequestration within a protective water ice host.

INTRODUCTION

Most scientists believe that terrestrial life as we know it originated on the Earth. However, observations made over the past 30 years suggest that many of the organic compounds antecedent to life could not have formed on the pre-biotic Earth. The early Earth is now thought to have had a more oxidizing atmosphere of CO_2, rather than the CH_4 atmosphere postulated earlier. The primitive oceans, rather than being a "primordial soup" were in all likelihood much more dilute, incapable of sustaining chemical reactions of sufficient variety or quantity for pre-biotic organic syntheses. Scientists now believe that much of the early prebiotic organic chemistry in fact took place in the extraterrestrial environment - within ices in the cold molecular cloud which collapsed to form the early solar nebula, and in icy and rocky planetesimals (the source material of comets and asteroids/meteorites, respectively) of the outer solar nebula.

Three sets of observations provide evidence that organic compounds exist in great quantity in the extraterrestrial environment. First, analyses of the Murchison and Allende carbonaceous chondrite meteorites, which fell to Earth in 1969, reveal

---

David F. Blake, Exobiology Branch, NASA Ames Research Center, Moffett Field, CA 94035-1000 USA, dblake@mail.arc.nasa.gov

abundant organic compounds. A list of these compounds is shown in Table 1. The parent bodies of these meteorites, which are among the most primitive and ancient objects in the solar system, must have either accumulated from materials containing these organic compounds, or the compounds themselves must have been synthesized in the parent bodies early in their history. Second, remote telescopic observations in the infrared and radio wavelengths show that simple organic compounds exist in abundance within cold molecular clouds (Table 1). Third, spectral analyses of chemical species present in the gaseous outflow of comets reveal a variety of simple organic species (Table 1). These species must have been frozen as simple ices in the cometary nucleus which volatilized upon warming.

THE ORIGIN OF THE BIOGENIC ELEMENTS AND THEIR FIRST ASSOCIATION WITHIN INTERSTELLAR ICE

OVERVIEW

Mixed ices containing mostly water are primary components of cold interstellar molecular clouds which are the birthplace of stars and protoplanetary nebulae (see Figure 1). This interstellar ice represents the earliest and most primitive association of the biogenic elements. Frozen on sub-micron-sized silicate grains, water ice serves as a matrix for the low-temperature (15-50 K) trapping of a variety of small carbon-bearing molecules. Exposure to UV radiation forms highly reactive free radicals which upon warming recombine to create a refractory organic residue. Laboratory simulations of the growth, radiation processing and thermal annealing of astrophysical ice analogs show that a variety of organic molecules can be synthesized, including complex hydrocarbons, alcohols, amines, nitrides, and esters or ketones as well as organic acids (Table 2). Remote infrared observations demonstrate that these organic compounds can exist in the interior of interstellar molecular clouds for long periods of time at ultra-low temperatures (10 - 20 K), protected from high particle or radiation fluxes by the bulk of the cloud itself.

Most low melting point solids were volatilized during gravitational collapse within the cold molecular cloud which formed our solar nebula. However, in the outer solar nebula, original icy condensates from the parent cold molecular cloud may have persisted or may have been volatilized and recondensed to form new ices representative of the early outer solar nebula. These condensates coalesced to form icy planetesimals (the parent bodies of comets) which now reside in the Oort cloud and the Kuiper belt. Early in solar system history, some of these icy planetesimals bombarded the volatile-poor rocky planets of the inner solar system, and thus provided the Earth with its rich complement of gases, volatiles, water, and biogenic elements and compounds.

Cometary bodies (Figure 2) are the most pristine and primitive objects in the solar system, possibly containing relict biogenic compounds and frozen volatiles from the parent molecular cloud. Thus, if one could deduce the physical and chemical state of components and phases within a cometary nucleus as it exists and can be observed today, insight could be gained into the nature of the volatiles and biogenic compounds introduced to the Earth ~4 billion years before the present.

Table 1a

Concentrations and Molecular Characteristics of Soluble Organic Compounds in Meteorites [73]

Class	Concentration (PPM)	# Compounds identified	Chain Length
Amino Acids	60	74	C_2-C_7
Aliphatic hydrocarbons	>35	140	C_1-C_{23}
Aromatic hydrocarbons	15-28	87	C_6-C_{20}
Carboxylic acids	>300	20	C_2-C_{12}
Dicarboxylic acids	>30	17	C_2-C_9
Hydrocarboxylic acids	15	7	C_2-C_6
Purines and Pyrimidines	1.3	5	NA
Basic N-heterocycles	7	32	NA
Amines	8	10	C_1-C_4
Amides	55-70	>2	NA
Alcohols	11	8	C_1-C_4
Aldehydes & Ketones	27	9	C_1-C_5
Total	>560	411	

Table 1b

Organics Detected in Astrophysical Ices [73-76]

Molecule	Cometary* Abundance	Interstellar Ice* Abundance
H_2O	100	100
CO (in polar ice)	5-10	1-10
CO (in non-polar ice)	~	10-40
CH_3OH	1-5	<4-10
CO_2	3	1-10
XCN	.1	1-10
H_2	~1	~1
CH_4	0.2-4.5	~1
HCO		~1
H_2CO	0-5	1-4
NH_3	0.1-2	1-4
N_2	~0.02	10-40
O_2	10-40	10-40
O_3	few	few
OCS or CO_3	few	few

*Molar concentrations relative to water ice

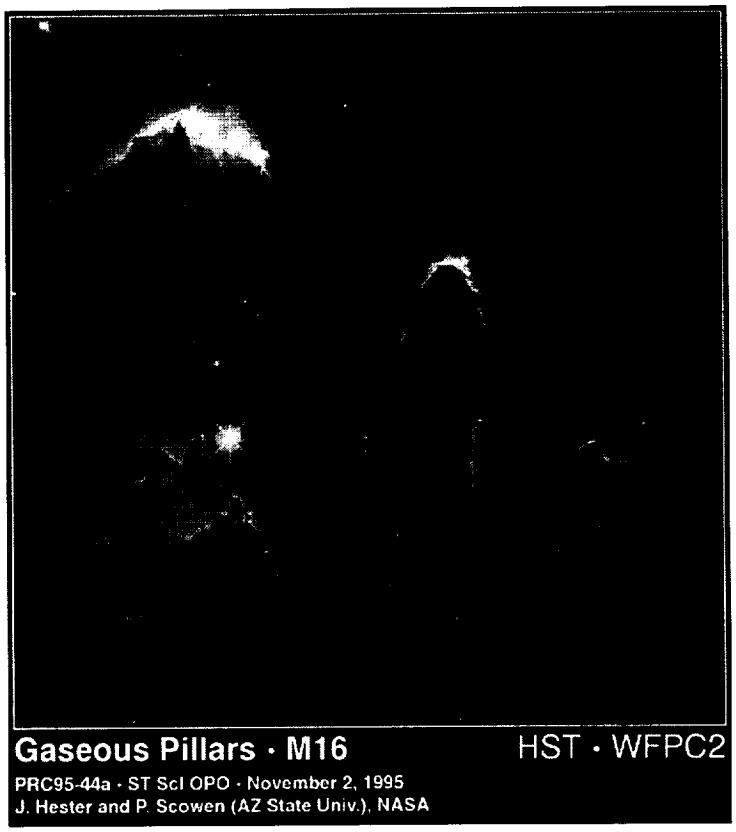

Fig. 1. Gas Pillars in M16 the Eagle Nebula. The dark pillar-like structures are columns of cool interstellar hydrogen gas and dust that are incubators for new stars. Inside cold molelcular clouds such as these, water-rich ices are condensed as thin rinds onto sub-μm dust grains. These interstellar ices represent the most primitive association of the biogenic elements, and are the sites of the first organic syntheses. Credit: Jeff Hester and Paul Scowan (ASU) and NASA.

Much of our present knowledge of the composition of interstellar ices is due to detailed laboratory studies of the growth and thermal and UV processing of mixed ices. These studies consist primarily of fingerprint-style matching of astronomical IR spectra with laboratory IR spectra from astrophysical ice analogs. The physics of cometary behavior has been studied by IR and gas release studies of analog ices as well as by direct observation of cometary behavior in the IR and radio wavelengths. This work has allowed scientists to infer the composition of various icy bodies and/or to explain on a phenomenological basis the outgassing events which are associated with coma formation.

However, a knowledge of the *petrology* (structure, phase relationships, microstructural associations and assemblages) of cometary and astrophysical ice analogs is fundamentally important because such physical properties underlie and control chemical reaction rates, volatile retention and release, vaporization behavior, thermal conductivity, bulk density, infrared spectral characteristics and so on. For solid phases it is really the structure of the icy materials which we would like to determine. Once structures are known, one can predict, correlate or explain in a fundamental way remote observations of real astronomical objects. In the research described herein, the detailed structure of crystalline and amorphous ices is determined directly by electron diffraction and related to other laboratory and astronomical observations.

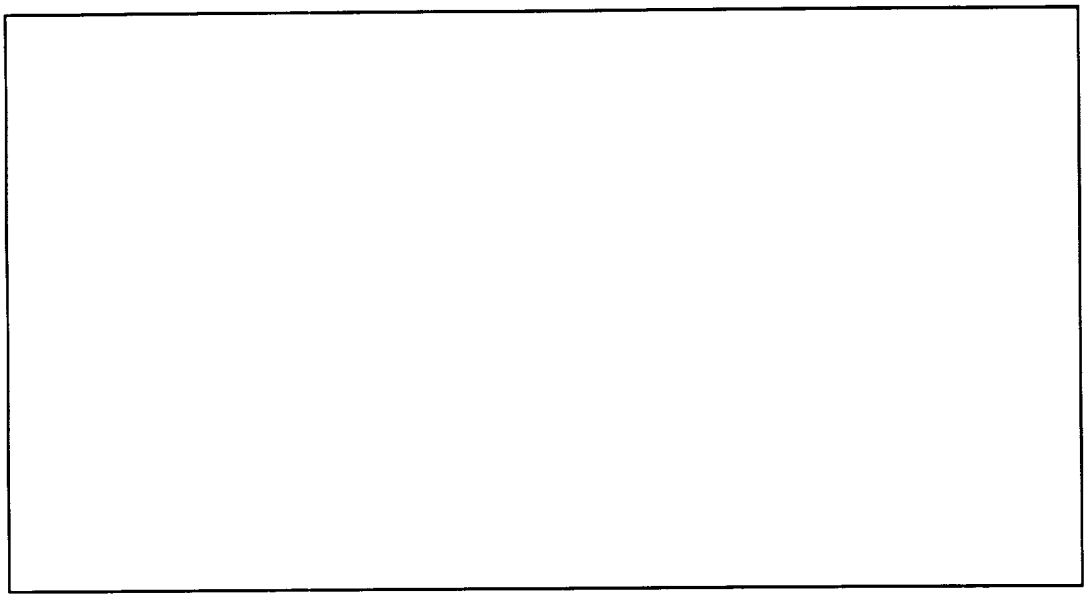

ICE IN THE INTERSTELLAR MEDIUM

Cold molecular clouds, the birthplace of stars and planetary nebulae, are dynamic environments in which small molecules exist both in the gas phase and as solid phases (principally water-rich ices) condensed onto small silicate and carbon grains. Gas phase molecules are observable through milimeter and sub-milimeter radio wavelength observations [1-3]. Using interferometry techniques, images with a resolution of 100-1000 AU (one astronomical unit is the distance from the Sun to the Earth) can be obtained which allow the investigation of temperature and gas composition within some star forming regions. Solid phase molecules, usually in the form of water-rich ice mantles on grains, are observable through infrared (IR) absorption measurements against a background illumination source, such as a star embedded within a cold molecular cloud [4-6].

Gas phase abundances can be modelled using gas phase ion-molecule reaction schemes. However, these reactions are found to be insufficient to explain the observed data of some species, indicating that small molecules are continually replenished from the solid state reservoir (i.e., from volatile-rich icy grains). The occurrence and abundance of gas phase molecules, in combination with short accretion timescales in cold molecular clouds, imply that a fast (~10^5 year) gas phase replenishment occurs [7,8]. This replenishment involves outgassing of ices and desorption of molecules, both determined by the structure of the solid host which is usually H_2O. A great deal has been inferred about the bulk composition and chemistry of ice in molecular clouds from laboratory studies of astrophysical ice analogs [5, 9-19]. These laboratory studies are continuing and expanding in response to the availability of recent IR astronomical observations of clouds as well as data from the Infrared Space Observatory.

The emphasis has traditionally been on IR spectral data which can be used for "fingerprint" matching of observed absorption bands in cold molecular clouds. However, IR spectroscopy does not have the capability to deduce structural or phase information from materials in the solid state, although typically such information is

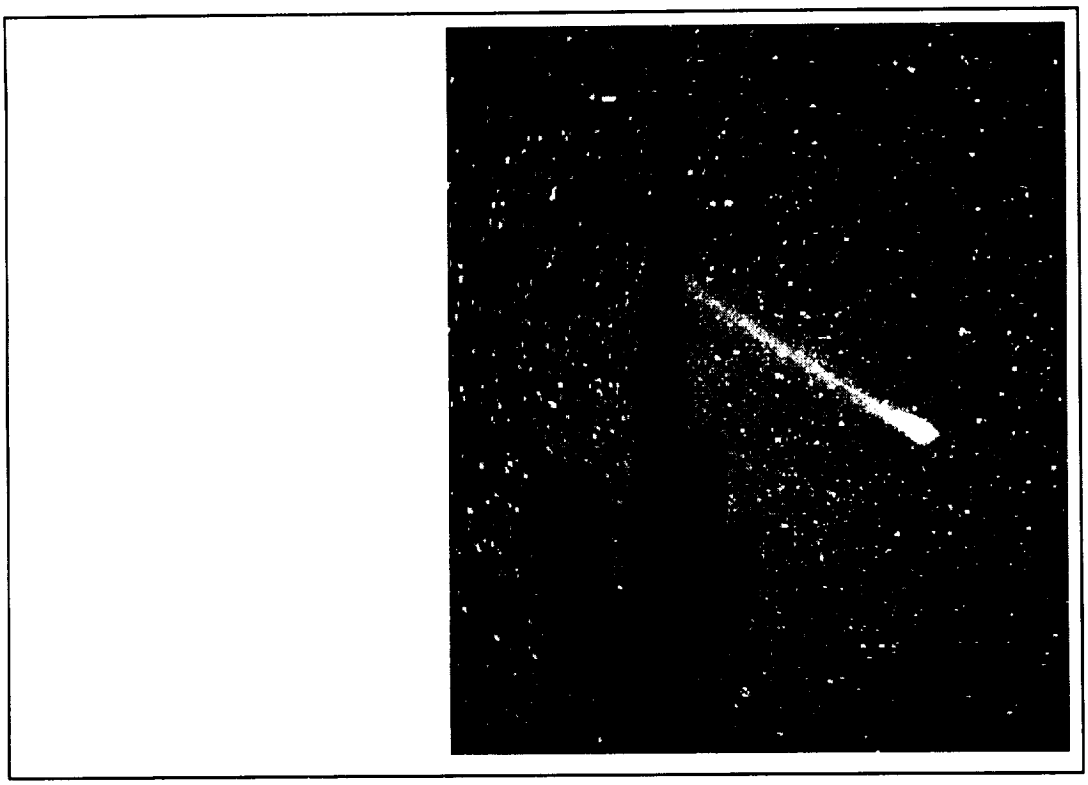

inferred indirectly to interpret the data. It is necessary therefore to utilize a structure-sensitive technique (i.e., X-ray, neutron or electron diffraction) in laboratory studies of astrophysical ice analogs in order to understand or deduce the mechanisms underlying the observed phenomena.

THE INTRODUCTION OF WATER ICE, ORGANIC MOLECULES AND VOLATILES INTO THE EARLY SOLAR NEBULA AND TO THE EARTH

Most low melting point solids such as water ice were volatilized during cloud collapse and the formation of the solar nebula. However, in the outer solar nebula, original icy condensates from the parent cold molecular cloud either persisted unchanged, or volatilized and recondensed to form new ices representative of the early outer solar nebula. These condensates coalesced to form icy planetesimals which became a part of the Oort cloud and the Kuiper belt. The Oort cloud is a spherical region of space extending from 1000 - 30,000 AU, beginning far beyond Pluto and continuing to halfway to the nearest star. The region is believed to contain millions of icy objects 1-50 km diameter, in highly elliptical orbit about the sun. These objects were formed near the present orbit of Jupiter, and cast out of the inner solar sytem by Jupiter's gravity [20]. The Kuiper belt is a ring-shaped region just outside the orbit of Pluto also believed to contain millions of icy objects. Kuiper belt objects, unlike Oort cloud objects, are thought to have remained at the same distance from the sun since their formation [20].

The inner rocky planets of the solar system, Mercury, Venus, Earth and Mars, are believed to have been devoid of volatiles at the time of formation of the Oort cloud

and the Kuiper belt - due to the high temperatures experienced at this distance from the proto-Sun. However, early in solar system history, a large number of icy planetesimals bombarded the volatile-poor rocky planets of the inner solar system, and in all likelihood provided the Earth with its rich complement of gases, volatiles, water, and biogenic elements and compounds. The evidence for this late bombardment, a period of intense cratering early in solar system history, had been largely circumstantial until lunar rocks were dated, and the cratering histories of the Moon, Mars, and moons of other planets were assembled. The Earth, having a plate tectonics cycle as well as a cycle of weathering, has retained almost no record of this early bombardment.

THE IMPORTANCE OF STRUCTURAL DATA FOR EXPLAINING WATER ICE BEHAVIOR

LABORATORY STUDY OF ASTROPHYSICAL ICES

The study of volatile release from amorphous and crystalline water ice has direct application to cometary and planetary outgassing phenomena as well as to studies of the thermal properties of astrophysical ices. Several investigations report anomalous gas release or vaporization phenomena which are as yet only poorly understood. For example, [21, 22] have described 8 different temperature regimes of gas release in water ice as it is warmed from 16° K to melting, yet water undergoes only 2 phase transitions in this temperature range. Two (possibly three) of the temperature regimes of gas release which occur below the amorphous to crystalline transformation suggest that changes in morphology, porosity, or short range local order ("annealing") are occurring even in the amorphous state. Sandford and coauthors [23] report different physical trapping mechanisms for different H_2O:CO ratios in their ices based on a detailed analysis of the fine structure of infrared spectra. Kouchi [24] studied the vapor pressure of amorphous and crystalline ices, and found an apparent two order of magnitude increase in vapor pressure for amorphous ice relative to crystalline ice at the same temperature. These data were used to explain the gas production rate of new comets vs. old. Kouchi and Kuroda [25, 26] studied the gas release and crystalline structure of low temperature mixed ices. Kochan and coauthors[27] report results from the KOSI experiments, in which large amounts of cometary ice analogs are grown and processed by heat and irradiation to release gases. Hsuing and Roessler [28] in their analyses of these simulated cometary nuclei from the KOSI experiments, report phase separation and migration of frozen volatiles within the ice. However, the original ices for the KOSI experiments were formed by spraying water and dust into liquid nitrogen. Under these conditions, the resulting ice is in its high temperature hexagonal form and the results are not directly applicable. Other studies [29-31] have been performed which address the presence or absence of ice clathrates in solar system objects and in laboratory analogs. The presence or absence of clathrates bears strongly on the physico-chemical nature of the ices and their structural and gas release properties. However the only direct proof of the presence of an ice clathrate is by analysis of structural data contained in diffraction patterns.

STRUCTURAL STUDIES OF ASTROPHYSICAL ICE ANALOGS

Nearly all of the laboratory studies of astrophysical ice analogs carried out to date record secondary or tertiary manifestations of structural or morphological change rather than observing such changes directly. While this approach is useful in mimicking the bulk physical and chemical phenomena taking place in cometary and other extraterrestrial ices, it does not reveal the mechanisms which control such phenomena. This phenomenological interpretation of data is probably the cause of somewhat contradictory explanations invoked to account for differences in behavior in similar temperature regimes. Furthermore, even in the case of [25, 26], structural data obtained by reflection electron diffraction are integrated over large volumes of ice relative to the size of individual crystallites. Thus, these structural studies do not reveal crystalline imperfections and cannot be used to characterize microstructural relationships, grain size, crystallite orientation and shape, grain boundary effects and inter- and intracrystalline defects. It is this microstructural, micromorphological and microchemical heterogeneity which must be characterized if the mechanisms underlying the observed phenomena are to be understood.

In order to elucidate the *mechanisms* responsible for the phenomenological observations described above, direct determinations of the structure and composition of astrophysical ice analogs prepared under realistic conditions are required. These analyses should be obtained at or below the level of resolution of individual crystallites within the ices (< 5 -100 nm). It is highly desirable to image individual domains of short-range order within amorphous ices (if they are present), to observe nucleation and growth phenomena from the vapor state onto grain surfaces, to follow structural changes during temperature-induced annealing, and to view the ices at high resolution during entrapped gas release phenomena. Likewise, it is desirable to study, at high resolution, the structural state, morphology, and microchemistry of mixed ices below, at, and above all of the temperatures at which subtle IR spectral features (attributed to different local ice "architecture;" see [23]) appear or change.

ELECTRON MICROSCOPY OF WATER ICE

LOW-PRESSURE FORMS OF WATER ICE

Water ice at low pressure can exist in three metastable amorphous forms, one metastable crystalline polymorph, and one stable crystalline polymorph. Amorphous water ice was first described early in this century. Diffraction studies were first performed by Burton and Oliver [32]. Low-density amorphous water ice (I_{a_l}) occurs when water vapor is deposited slowly onto an inert surface at 77 K. I_{a_l} has a density of 0.94 [33-35] and has been extensively studied because of its similarity to liquid water [36-39], and because it can be used as an embedding medium for biological tissues observed in electron microscopy [40-42]. High-density amorphous water ice

(Ia_h) was first reported by [34]. X-ray diffraction patterns of water vapor deposited onto a substrate cooled to 10 K showed the presence of oxygen atoms at distances between those of the first and second nearest neighbor at the interstitial site of the Ia_l structure, which results in a higher value for the calculated density of oxygen atoms (i.e., 1.1 instead of 0.94). For this reason, Narten and coauthors [34] introduced the names "high density amorphous ice", (Ia_h) and "low density amorphous ice" (Ia_l). Subsequent experiments failed to reproduce the high-density form and from this it was concluded that the high density amorphous form was an artifact of epitaxial growth on an oriented single crystal [37, 43-44]. Later it was shown that high density amorphous ice can form during vapor deposition on amorphous carbon films [41, 45]. Another form of high density amorphous water ice can be made by pressure melting, and is also referred to as high-density amorphous ice (hda or HDA). When cooled to 77 K, crystalline hexagonal ice, Ih, undergoes a transition into hda at 1-2 GPa pressure [46, 47]. The resulting ice has a density of 1.17 and can persist metastably for some time at low pressure and 77 K. When this pressure-induced high density amorphous ice is warmed the ice transforms irreversibly into low density amorphous ice in the range 105-123 K [46, 48-51]. The radial distribution function of hda [49,52] differs significantly from that of the Ia_h of [34] and it has been argued that pressure-induced hda has more hexagonal order than vapor-deposited Ia_h [53].

When amorphous water ice is warmed to a high enough temperature, the ice crystallizes into the cubic crystalline polymorph (Ic, space group Fd3m) before, at higher temperatures, recrystallization to the stable hexagonal crystalline polymorph (Ih, space group $P6_3/mmc$) occurs. Prior to cubic crystallization, amorphous water ice undergoes a weak glass transition that manifests itself as an endothermic step in differential thermal analysis (DTA) scans [54-57]. During this transition, the amorphous solid transforms into a viscous liquid. During the crystallization process, a significant amount of amorphous water ice persists as a third amorphous form which has a slightly different structure than Ia_l [33,45]. This form of amorphous water ice is called the "restrained amorphous form" (Ia_r) because it apparently inhibits crystallization into the cubic crystalline polymorph.

The cubic crystalline polymorph (Ic) can result from warming amorphous ice through the amorphous - cubic ice transition temperature (120-140 K, time-dependent), from direct deposition of water vapor onto a substrate in the temperature range 130-150 K, or from direct deposition of water vapor onto a substrate at temperatures <120 K, due to heat of fusion, if deposition rates are rapid enough. In fact, crystallization to Ic (as a consequence of heat of fusion) during vapor-deposition at T<120 K occurs in all but the slowest deposition experiments, with the result that making bulk quantities of low-density amorphous water ice in the laboratory is not possible.

The hexagonal crystalline polymorph results form the cooling of liquid water below the freezing point, from the vapor-depositon of water above ~160 K, and from the warming of cubic crystalline ice above ~230 K. The hexagonal crystalline polymorph is the most common form of water ice on the Earth, manifesting itself in the familiar form of snowflakes.

ELECTRON MICROSCOPY OF ASTROPHYSICAL ICE ANALOGS

A brief description of the modifications required to deposit, image and process astrophysical ice analogs in an Electron Microscope is given in [58]. The instrument is shown in Figure 3. Modifications were made to the microscope to accomplish two purposes: First, vacuum system modifications were made to reduce the partial pressure of water vapor and hydrocarbons by several orders of magnitude so that vacuum-born sample contamination is substantially reduced. Second, a low electron dose system was fabricated and installed with the intent of minimizing damage to electron beam sensitive samples. Images are collected digitally using a cooled, slow scan CCD camera and processed using a commercial image processing program. A gas inlet tube was installed so that gases of selected compositions could be leaked into the sample chamber and vapor-deposited on a cooled sample substrate. A Quadrupole Mass Spectrometer was interfaced directly into the objective lens polepiece and is used to monitor gas deposition conditions, and to record pressure changes for up to 12 masses during the course of an experiment.

Samples are introduced into the electron microscope in two ways: (1). Ices collected or grown elsewhere can be inserted into the microscope in the frozen state using a cryotransfer device. The liquid nitrogen stage used for cryotransfer operates in the range 100-373 K. It has a cryoshutter which allows the sample and specimen rod to be taken out of the microscope while at low temperature. Frozen samples can be loaded and unloaded from the stage inside a cryotransfer station and transported at liquid nitrogen temperatures in special dewars. (2). Ices can be grown *in situ* by leaking pre-mixed gases directly onto a cold sample substrate inside the microscope. The specially fabricated liquid helium cooled stage is equipped with a shutter to protect the specimen during extended periods of annealing. A heater control allows temperatures between 15 and 373 K.

The substrates for ice deposition are ~5 nm thick carbon films supported by 400 mesh Cu electron microscope grids. A typical *in situ* deposition and annealing experiment proceeds as follows: A sample bulb filled with water vapor or other gas mixtures at reduced pressure (1 -20 Torr) is placed on the microscope, and the sample insertion lines are evacuated. The cryostage is then put in the microscope and cooled to the desired starting temperature. While the sample substrate is being viewed at low magnification, the gas is leaked into the chamber surrounding the substrate surface. A needle valve is used to control the flow of gas into the sample chamber and the resulting vapor deposit of ice is monitored by inspection. Ice can be deposited at the rate of nanometers per hour to microns per hour. The sample substrate can be tilted directly toward the gas inlet (for ballistic deposition), or oblique to the inlet so that molecules must diffuse indirectly to the substrate. The latter method of deposition disallows the formation of water clusters due to supersonic flow, as described by [59].

Figure 4a shows an electron diffraction pattern from the ice which indicates that it is amorphous at the level of electron diffraction (some short-range order is certainly present, but no trace of crystallinity is evident in the pattern). The sample is warmed up slowly and diffraction patterns are taken at regular intervals of temperature. Figure

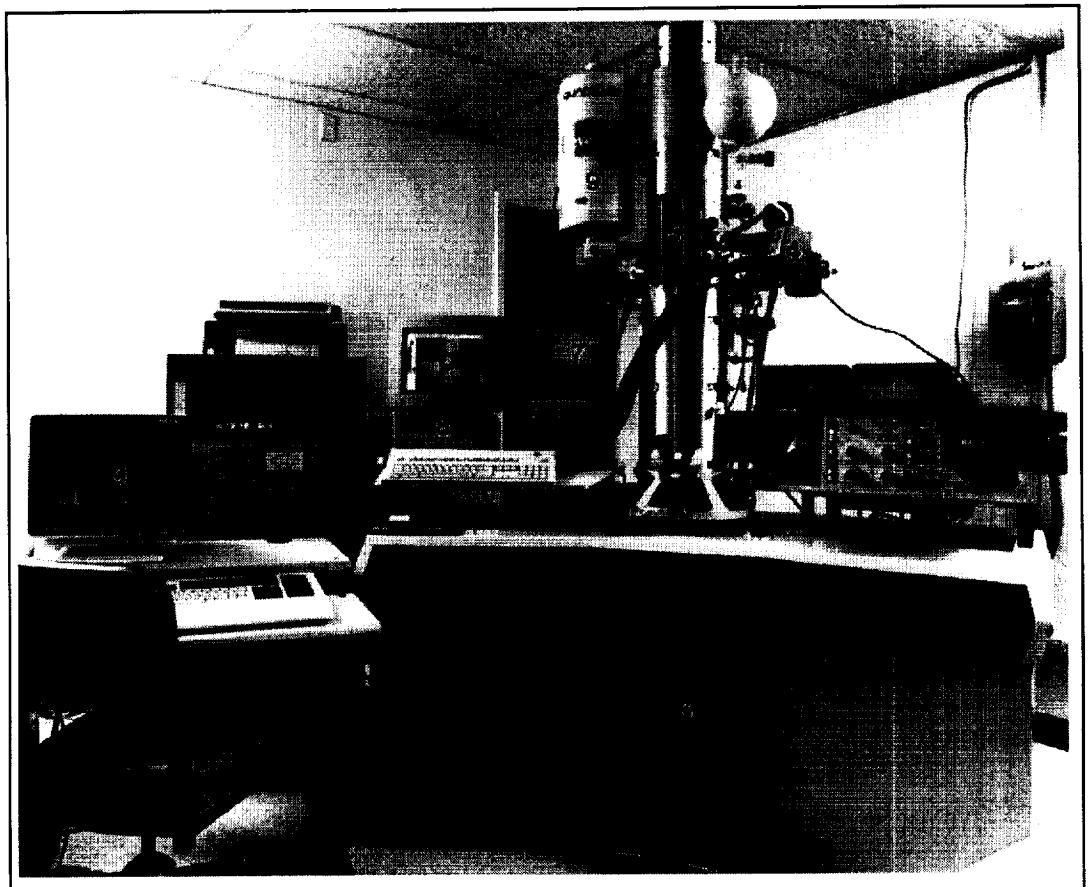

Fig. 3. Electron Microscope, modified for high vacuum and low electron-dose imagery of ices. (1). Gas bulb used to leak pre-mixed gases onto the sample substrate inside the microscope. (2). Gas inlet valve, which can be used to adjust the rate of deposition of ices from nanometers per hour to microns per hour. (3). Cryogenic sample holder, capable of temperatures from 15-363 K. (4). Quadrupole mass spectrometer used to record mass spectra from gases released during thermal annealing. (5). Ion pump which, in concert with a LN_2 anticontamination device, maintain a low-10^{-7} torr vacuum at the sample. (6). Digital camera with image intensifier for recording low-dose images of ice. (7). TV monitor for real-time viewing of images and diffraction patterns. (8). Computer for recording and analyzing digital images and diffraction patterns in real time.

4b shows the first indication of the amorphous to cubic transition ($Ia_r \rightarrow I_c$). The arrow in the figure marks the first indication of an I_c 220 maximum. This transition occurs at 143° ± 2° K, which is (within error) the transition temperature reported in the literature [40]. However, as we will show later, the temperature of onset of cubic crystallization is a sensitive function of annealing time and the rate of warming of the ice, and may vary by as much as 20-30 degrees, depending on temperature history. Figures 4c and 4d show further increases in crystallinity.

In addition to viewing electron diffraction patterns and recording them electronically, it is also possible to record moderately high resolution images at low electron dose in order to view the morphology and defect structure of individual crystals and aggregates at nanometer resolution. In crystalline samples, it is possible to view the size, shape, and degree of perfection of individual crystallites by using bright and dark field imaging. Figure 5a shows a selected area electron diffraction

pattern for hexagonal ice obtained from water vapor deposited at 160° K. Figure 5b shows a cubic diffraction pattern, obtained from water vapor deposited at 140° K. By tilting the electron beam so that different parts of the diffraction pattern are allowed to pass through the objective aperture, bright and dark field images are formed. Figure 5c for example, is a bright field image of cubic ice, obtained by directing the central beam through the aperture (position labeled as "a" in Figure 5b). Figure 5d shows a dark field image from the same area, obtained by placing the aperture in the position labeled "b" in Figure 5b. By careful dark field tilting experiments, it is possible to identify the types of defects in individual ice crystallites, as well as to determine their orientation, size and shape.

REAL-TIME ELECTRON DIFFRACTION AND COMPUTER REDUCTION OF PATTERNS

The phase changes and structural annealing which take place in amorphous and crystalline water-rich ices are critically dependent on time and temperature. In gas release and IR studies of ice, the rate of data collection is typically not a limiting factor in an experiment (that is, spectra can be recorded rapidly enough to identify changes as they occur). However, for conventional analysis using X-ray diffractometry, a single high resolution pattern may require hours of intergration time. In the classic

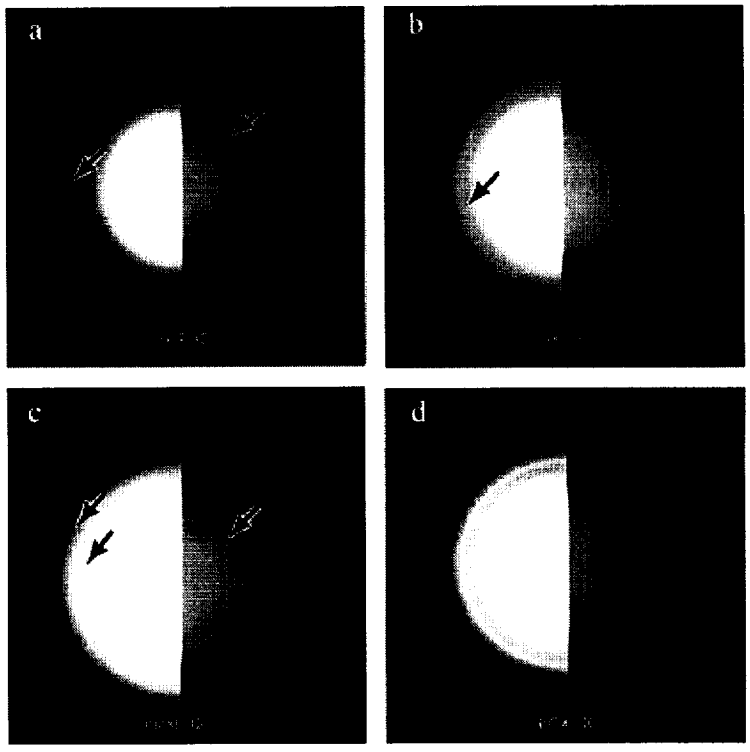

Fig. 4. Electron diffraction patterns of low-temperature water ice. (a). Diffraction pattern of a 10μm diameter region of amorpnous ice which was vapor deposited at 100 K and warmed to 133 K. Note the two diffuse maxima (arrowed) but no sharp maxima indicative of crystalline ice. (b). diffraction pattern of amorphous ice recorded at 143 K at the onset of the amorphous to crystalline cubic ice transition. The arrow shows a sharp band of intensity at the position of the 220 maximum of cubic ice. (c). Diffraction pattern recorded at 153 K showing the increase in crystallization of the cubic phase. (d). diffraction pattern recorded at 163 K showing further transformation to cubic ice. It is noteworthy that the amorphous ice never fully transforms to the crystalline state until complete recrystallization into the hexagonal polymorph.

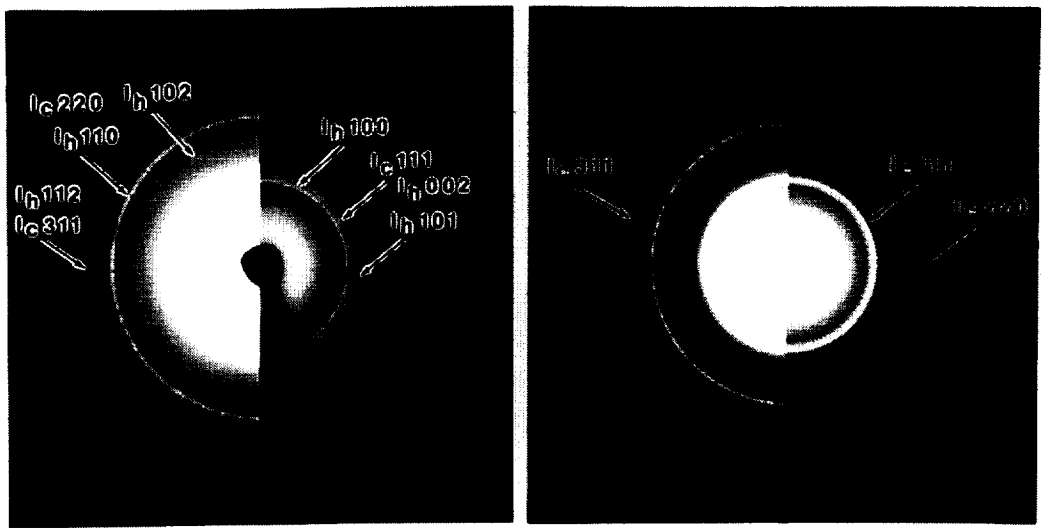

work of Narten and coauthors [34] for example, ice samples were deposited over a period of 2 weeks, and structural interpretations were based on only 4 diffraction patterns. In our experiments the temperature is increased at the rate of 1 K per minute (analogous to typical IR experiments), and it would be desirable to be able to collect patterns at the rate of at least one per Kelvin, over temperature ranges of 200 K. By conventional film methods, an electron diffraction pattern can be exposed in as little as 2 seconds, but the microscope only carries a small number of sheets of film per cassette. This quantity is insufficient particularly when one wants to bracket exposures and collect standardized patterns before and after the experiment is run.

Hardware and software improvements to the imaging system were made so that diffraction patterns could be collected on-line in real time. As a result, hundreds of patterns can be collected at the rate of one every few seconds, and stored electronically. Computer programs reduce the two-dimensional diffraction patterns (figure 6a) to one-dimensional radial intensity functions (figure 6b). These intensity vs. radial distance functions are calibrated using an internal crystalline gold standard which is sputtered onto a small portion of the support substrate, and an amorphous carbon background is subtracted to represent the 5 nm substrate. Then, an atomic scattering

background is subtracted to yield a diffracted intensity distribution in reciprocal space (figure 6c).

LOW-TEMPERATURE STRUCTURAL TRANSFORMATIONS IN WATER ICE

Figure 7 shows background-subtracted radial intensity distributions of ice diffraction patterns during warming from 15 to about 200 K. High density amorphous ice (Ia_h) forms when water is vapor deposited below about 65 K. This high density, low-temperature form of amorphous ice transforms irreversibly to low density amorphous ice (Ia_l) above about 65 K. Low density amorphous ice gradually transforms to cubic ice at 140-150 K. If one subtracts a pure crystalline cubic ice pattern from a crystallized amorphous ice pattern, the residual intensity resides in a third amorphous phase (Ia_r), which persists to higher temperatures (>190K) along with the crystalline ice. It is notable that no more than about 30% of the amorphous ice *ever* crystallizes. This has important implications for the volatilization of water and trapped gases from comets.

These patterns are striking, and reveal much about the dynamics of water ice. However, to interpret real-time data recorded using other techniques (IR, gas release, etc.), one needs to interpret the data more quantitatively. Computer software was

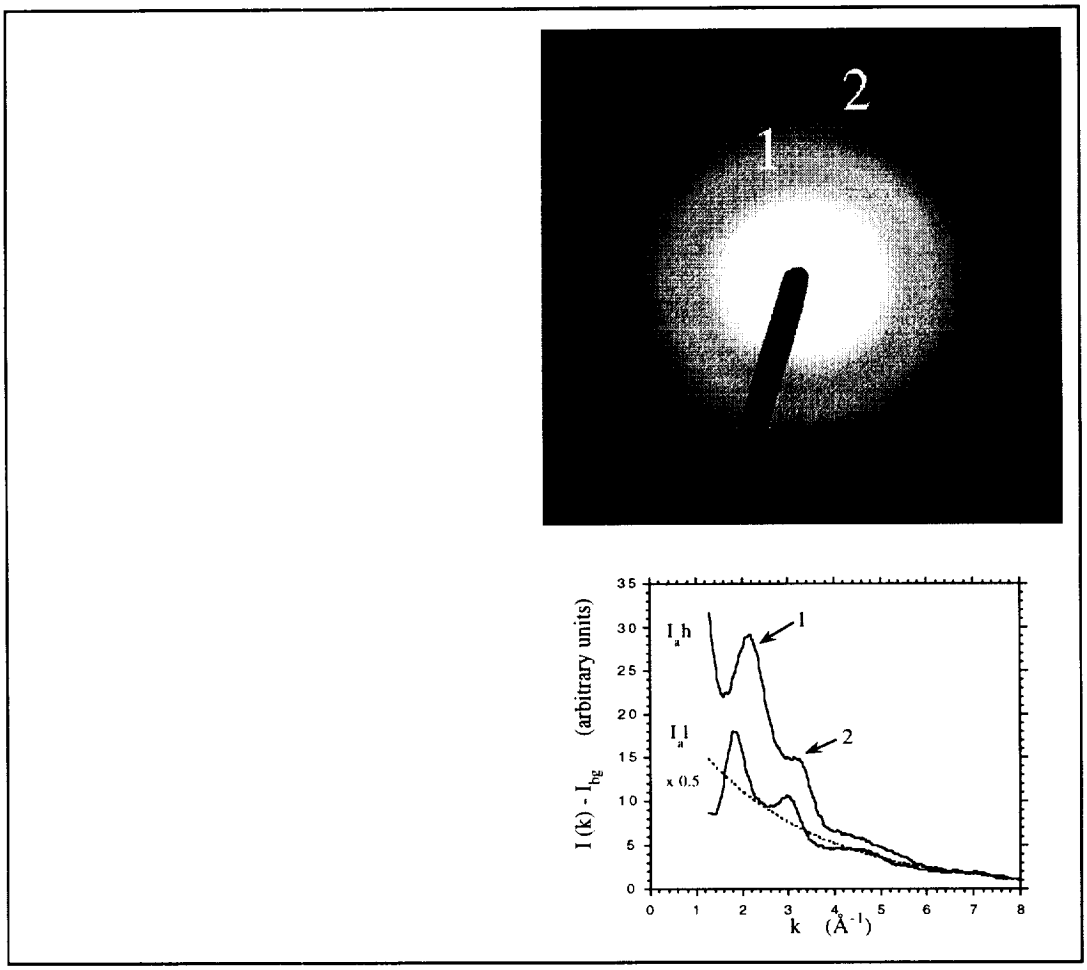

written which fits Gaussian curves beneath the two principal maxima in the amorphous water ice pattern. In this way, one can study small changes in the position, height and breadth of the peaks as a function of temperature or processing history. Two parameters of the amorphous diffraction maxima were found which reflect repeatable and substantive changes in the structure of the amorphous ice during warming. Figure 8a-b shows these parameters for a series of about 150 patterns recorded at 1 per K per minute during an experiment. Each data point in the figure represents a measurement of a particular feature of a particular diffraction maximum at a specified temperature. From these data one can quantify the transformation from one amorphous form to another and relate these changes to other real time changes. For example, the *position* of the first amorphous peak appears to faithfully reflect the transition of high density amorphous ice to low density amorphous ice ($Ia_h \rightarrow Ia_l$), which occurs between about 35 and 65 K. Changes in the *intensity* of the first amorphous peak reflect the transformation from the low density amorphous form to the restrained amorphous form ($Ia_l \rightarrow Ia_r$) between 130 and 150 K.

The $Ia_h \rightarrow Ia_l$ transformation between 35 and 65 K can be correlated with and indeed, underlies and explains other data, for example changes in the character of CO trapping sites [23], changes in the shape of the 3.07 μm water band as a function of temperature [60], or the temperatures at which radicals recombine in UV photolyzed ices to form organic compounds [61-62]. These and other conclusions are more fully explained in [45, 63]. These papers conclude that high density amorphous ice (Ia_h) is the most common form of ice in the universe, and that the $Ia_h \rightarrow Ia_l$ transformation

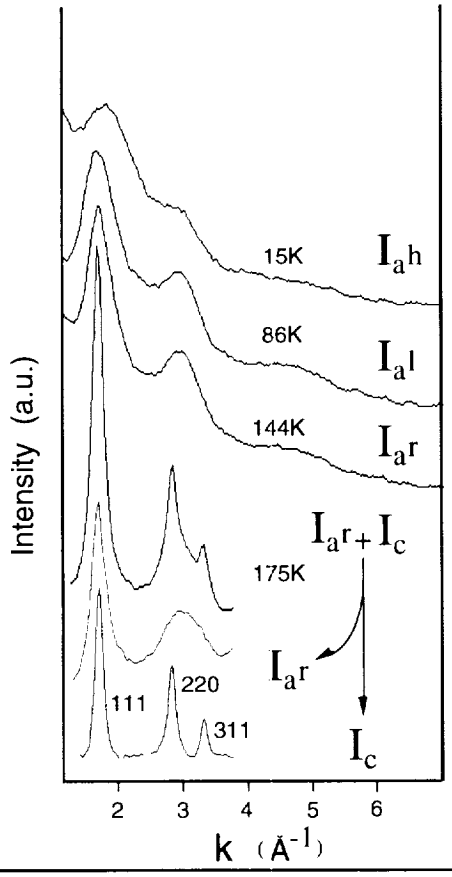

Fig. 7. Electron diffraction radial intensity distributions (diffractograms) of the different forms of vapor-deposited water ice from a region about 10 μm in diameter. The forms encountered are high-density amorphous ice (Ia_h), low-density amorphous ice (Ia_l), restrained amorphous ice (Iar) (while transforming from Ia_l), and a composite of restrained amorphous and cubic crystalline ice (Ic). The latter can be separated into two components by subtraction of a standard cubic pattern as indicated, which allows one to follow changes in the amorphous component after the onset of cubic crystallization (after [45]).

controls the recombination of biogenic elements to form organic compounds within interstellar ices. This research provides a physical basis for subtle changes in the 3.07 μm water band in astrophysical ice analogs and provides ground truth for the determination of the temperature and to some extent the thermal history of astrophysical ices. Small changes in the IR band structure of molecules trapped in the ice (e.g., CO), can be used to illuminate the structure state and thermal history of the parent ice. The $Ia_h \rightarrow Ia_l$ transformation has important implications for ices within cold molecular clouds as well as for ices within comets.

THE STRUCTURE OF AMORPHOUS WATER ICE; EXPERIMENTAL DATA AND MOLECULAR DYNAMICS SIMULATIONS

Fourier transformation of the diffraction patterns of amorphous water ice yields the radial distribution function (rdf) of distances between oxygen atom pairs [64, 65]. Figure 9 shows rdfs from our electron diffraction data along with X-ray diffraction data from pressure amorphosed ice [49], and X-ray diffraction data from vapor-deposited ice [34]. The high density form is characterized in all cases by a splitting of the second nearest neighbor peak such that one component lies between the first and second nearest neighbor peaks of the low-density amorphous form. Molecular dynamics calculations were made of the formation of amorphous water ice (details of

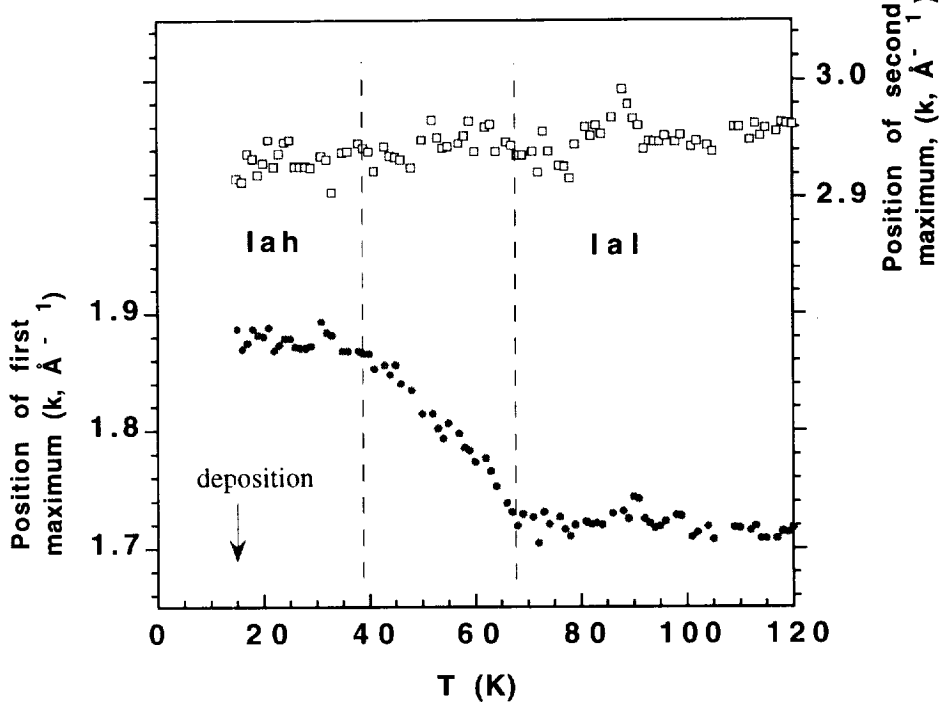

Fig. 8a. Temperature depencence of the position of the first and second diffraction maxima in the temperature range in which amorphous water ice transforms from the high-density form to the low-density form. The transition is well defined, but sluggish. The ice was vapor-deposited at 15 K and held for 37 minutes before warm-up at a rate of 2 K per minute (after [45]).

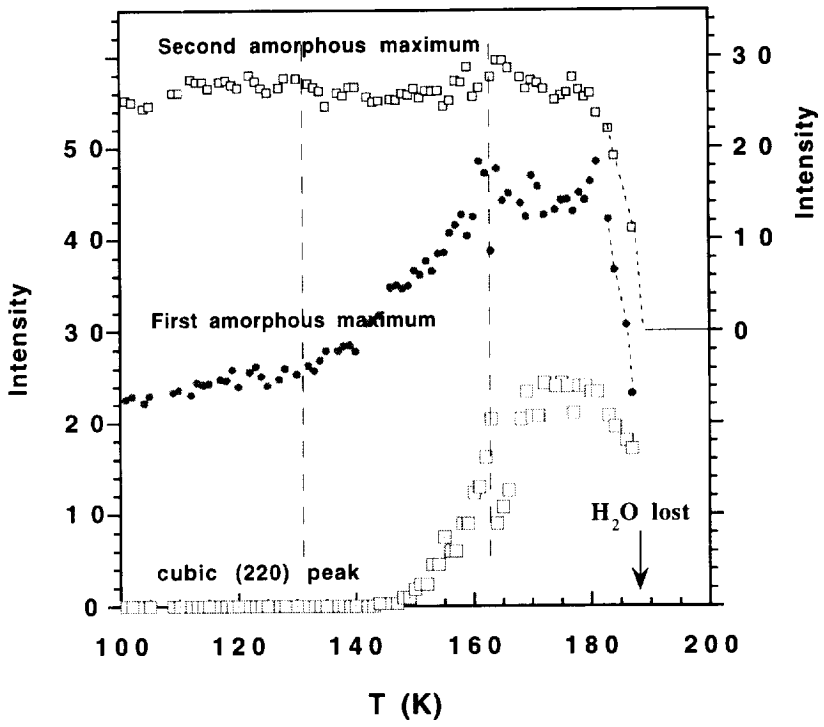

Fig. 8b. Temperature depence during warmup of the intensity (in arbitraty units) of, from top to bottom, the second and first diffraction peaks of the amorphous component and the cubic 220 peak, which marks the onset of crystallization into Ic. The onset of the transition $Ia_i \rightarrow Ia_r$ is well defined by an increase in intensity of the first diffraction peak. The heating rate was 1 to 2 K per minute, and the onset of the cubic crystallization occurred 182 min. after depositon at 15 K (after [45]).

this are shown in [63, 66]) and these results were compared with experimental data. The similarity in the rdf results suggests that the modeling correctly represents the ice deposition process. Once one is reasonably certain that the computer model of ice is a good stand-in for the real ice formed in the electron microscope experiment, the computer generated structure can be sampled to determine the average coordination number of the oxygens, the strength and number of hydrogen bonds per atom, the size of pore spaces in the structure, etc (e.g., see Table 3). The data appear to support the model of [50] in which the high density amorphous form is a collapsed low-density lattice, characterized by the presence of oxygen-oxygen distances between 3 and 4 Å.

Jenniskens and Blake [45] propose the existence of two fundamentally different types of cometary ice based on thermal history. Two families of comets are known: Kuiper belt objects, which remain during their lifetime at temperatures below 30 to 50 K, and Oort cloud objects, which were expelled from their formational zones in the Uranus-Neptune region where the ice was heated to some 60 to 100 K. After being expelled, Oort cloud comets cool down to temperatures T<20 K but retain the structural signature of their higher temperature origin. Kuiper belt objects should be

made of high density amorphous ice, whereas Oort cloud comets should be made of low density amorphous ice. The difference in ice structure may manifest itself in the outgassing characteristics of new comets.

HIGHER TEMPERATURE STRUCTURAL TRANSFORMATIONS IN AMORPHOUS WATER ICE AND ICE CRYSTALLIZATION

A second amorphous-to-amorphous transformation is seen in vapor-deposited amorphous ice (Ia_l) as it is heated to a temperature just below to the crystallization temperature (Figure 8b). This transformation results in a new form of amorphous water ice called the restrained amorphous form (Ia_r). The restrained amorphous form, as its name implies, resists crystallization, and indeed, persists metastably with cubic crystalline ice throughout its range. The onset of the $Ia_l \rightarrow Ia_r$ transition coincides with the glass transition (T_g) in water ice, a structural relaxation which marks the change from a solid to a viscous liquid [67, 68]. It is this transition, and not the crystallization of amorphous ice *per se*, which underlies the release of trapped gases and initiates many other processes (e.g., clathrate formation in impure ices; [69]) which occur in the temperature range 120-150 K. During the $Ia_l \rightarrow Ia_r$ transition, pore spaces are annealed out of the structure and residual dangling -OH bonds are eliminated. This results in the release of "excess volatiles" held in pore spaces, while the restrained amorphous ice is still capable of retaining at least 10 % volatile species until it volatilizes or is recrystallizes into cubic or hexagonal ice.

Structural data from time-temperature-transformation experiments indicate that no more than 30% of amorphous water ice ever crystallizes to the cubic polymorph below about 200 K [33, 45]. This resistance of Ia_r to crystallization is examined in [70] , where the first direct evidence is presented that amorphous water ice above its glass transition behaves as a "strong" liquid (Angell, 1993). Nucleation rates of cubic crystalline water ice within a Ia_r precursor are unlike those measured for liquid water clusters [71], suggesting that restrained amorphous ice is thermodynamically distinct from liquid water. The temperature dependence in the model that describes the liquid water clusters is too steep below T = 150 K to fit the nucleation rates for Ia_r. The behavior of Ia_r as a strong liquid manifests itself in the persistence of the amorphous form to high temperatures and its coexistence with cubic crystalline ice over long time periods. This anomalous behavior suggests that within cometary ices, the bulk of the ice volatilizes directly from the amorphous state rather than first crystallizing to cubic or hexagonal ice.

[72] pointed out that the "strong liquid" character of amorphous water ice above the glass transition can be modified by the incorporation of impurities. It is likely that Ia_r will have a differing viscosity-temperature relationships based on the nature and quantity of impurities in the ice. It is interesting to note that, if a more "fragile" liquid character is imparted to the amorphous ice due to impurities, the steep dependence of viscosity on temperature will result in the persistence of amorphous ice to higher temperatures or for longer periods of time.

Lastly, we note that there must be some structural cause for the "strong liquid"

character of Ia_r. What prevents Ia_r from fully transforming into cubic ice? The answer may be that Ia_r contains a recognizable short-range hexagonal stacking order which restrains the materials from crystallizing [45]. To form cubic crystals, the ice has to fully restructure all layers with ABAB (hexagonal) type stacking into ABCABC (cubic) type stacking. Domains with hexagonal short-range order probably resist restructuring into cubic short-range order and persist metastably until wholesale restructuring transforms all ice into the thermodynamically stable hexagonal polymorph at higher temperatures. Electron micrographs of amorphous water ice lend some insight. Figure 10 shows Ia_r coexisting with cubic ice after various annealing times. The inset diffraction pattern shows some hexagonal ice (Ih) maxima despite the fact that the ice is in the cubic temperature domain. Many of the crystallites in the image show planar defects, often separated by a few tens of Ångstroms, which we interpret to be stacking faults. These stacking faults are probably mistakes in ABCABC

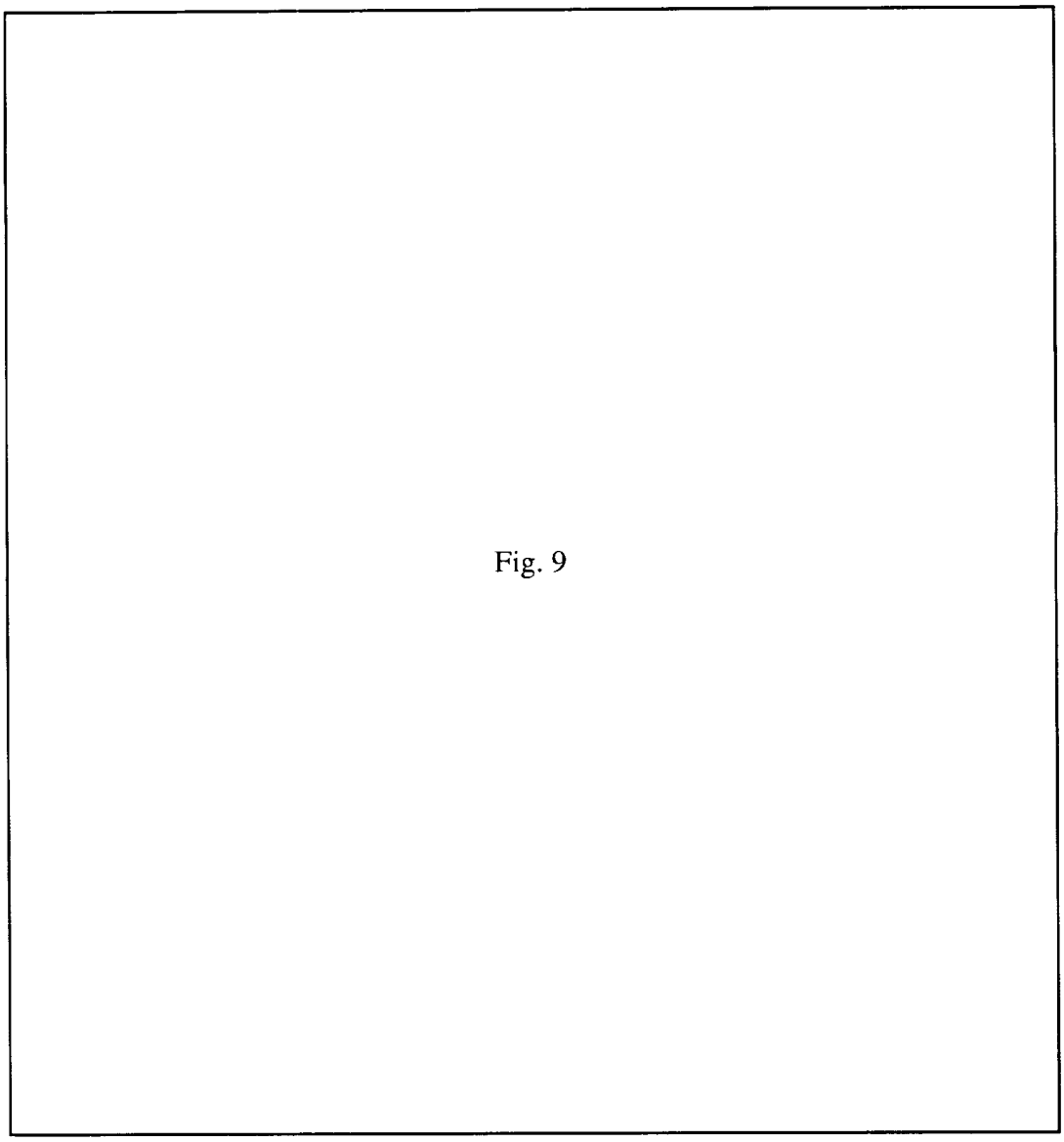

Fig. 9

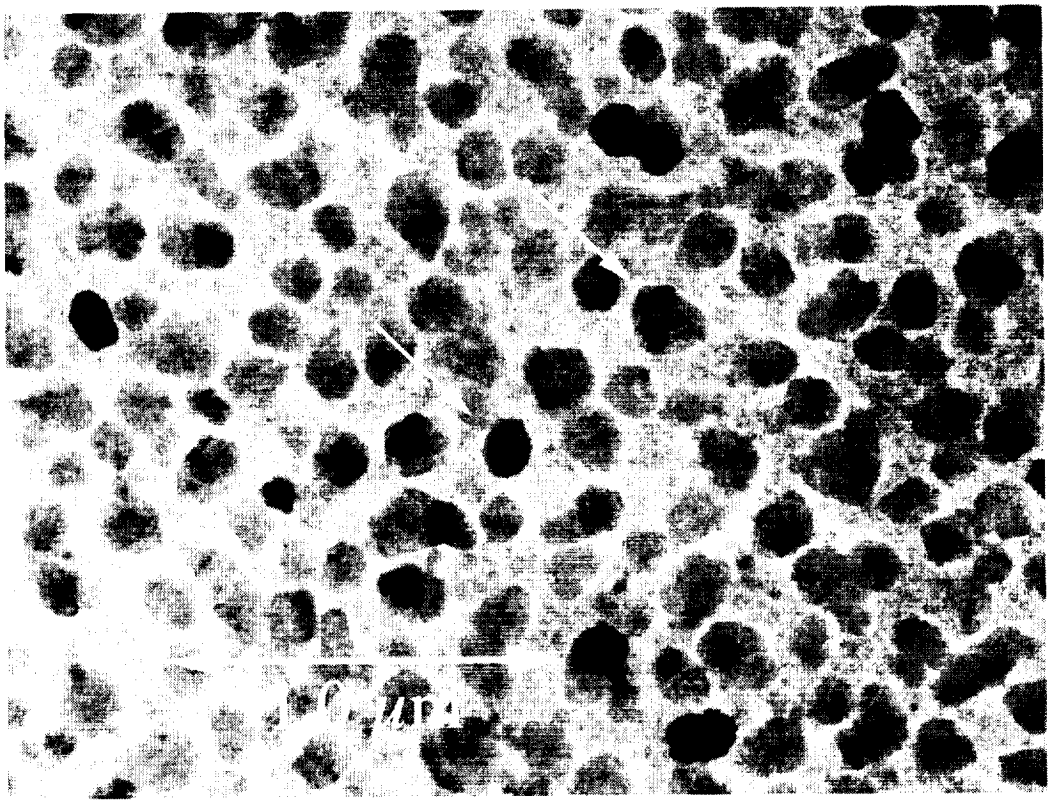

Fig. 10. Bright field image of water ice, vapor-deposited in the amorphous state and annealed to 132 K for 24 hours. Note individual crystals of ice, some showing planar defects with spacings less than 5 nm (arrowed). The defects are attributed to local stacking disorder in which the normal ABCABC... stacking sequence of the cubic polymorph is interrupted by hexagonal ABAB... planes.

ordering, which would result in small hexagonal domains in the ice.

REFERENCES

[1]. Mundy, L.G., H.A. Wootten and B.A. Wilking (1990). The circumstellar structure of IRAS 16293-2422: $C^{18}O$, NH_3, and CO observations. Ap. J. **352**, 159-166.

[2]. Mundy, L.G., A. Wooten, B.A. Wilking, G.A. Blake and A.I. Sargent (1992). IRAS 16293-2422: A very young binary system? Ap. J. **385**, 306-313.

[3]. Charnley, S.B., A.G.G.M. Tielens and T.J. Millar (1992). On the molecular complexity of the hot cores in Orion A: Grain surface chemistry as the "last refuge of the scoundrel. Ap. J. Lett. **399**, L71-L74.

[4]. Allamandola, L.J. and S.A. Sandford (1988). Laboratory simulation of dust spectra, in *Dust in the Universe* (M.E. Bailey and D.A. Williams, Eds.), Cambridge Univ. Press, Cambridge, 229-263.

[5]. Allamandola, L.J., S.A. Sandford and G.J. Valero (1988). Photochemical and thermal evolution of interstellar/precometary ice analogs. Icarus **76**, 225-252.

[6]. Allamandola, L.J., Max P. Bernstein and S.A. Sandford (1997). Photochemical evolution of interstellar/precometary organic material, in *Astronomical and biochemical origins and the search for life in the universe* (Eds. C.B. Cosmovici, S. Bowyer and D. Werthimer, Editrice Compositori, Bologna, 23-47.

[7]. Greenberg, J.M. (1977). in Liege Astrophysical Symposium on the Spectra of Small Molecules (Univ. of Liege: Liege), pp. 555.

[8]. Iglesias, E. (1977). The chemical evolution of molecular clouds. Ap. J. **218**, 697-715.

[9]. Hagen, W., L.J. Allamandola and J.M. Greenberg (1979). Interstellar molecule formation in grain mantles: The laboratory analog experiments, results and implications. Astrophys. Space Sci, **65**, 215-240.

[10]. Moore, M.H., B. Donn, R. Khanna and M.F. A'Hearn (1983). Studies of proton-irradiated cometary-type ice mixtures. Icarus, **54**, 388-405.

[11]. Strazzulla, G., V. Pirronello and G. Foti (1983). Physical and chemical effects induced by energetic ions on comets. Astron. Astrophys., **123**, 93-97.

[12]. Johnson , R.E., L.J. Lanzerotti, W.L. Brown, W.M. Augustyniak and C. Mussil (1983). Charged particle erosion of frozen voltatiles in ice grains and comets. Astron. Astrophys., **123**, 343-346.

[13]. Lanzerotti, L.J., W.L. Brown and R.E. Johnson (1985). Laboratory studies of ion irradiations of water, sulfur dioxide and methane ices. IN: Ices in the Solar System, eds. Klinger, J. D. Benest, A. Dollfus, and R. Smoluchowski, pp. 317-335. (NATO ASI series C 156.) LReidel, Dordrecht, The Netherlands.

[14]. d'Hendecourt, L.B. and L.J. Allamandola (1986). Time dependent chemistry in dense molecular clouds. III. Infrared band cross sections of molecules in the solid state at 10 K. Astron. Astrophys., Suppl. Ser., **64**, 453-467.

[15]. Johnson, R.E., J.F. Cooper and L.J. Lanzerotti (1986). Radiation formation of an non-volatile crust. 20th ESLAB Symposium on the Exploration of Halley's Comet. Eds., Battrick, B., E.J. Rolfe and R. Reinhard, ESA SP-250, Vol. II, 269-272. ESA Publications, ESTEC, Noordwijk, The Netherlands.

[16]. Thompson, W.R., B.G.J.P.T. Murray, B.N. Khare and C. Sagan (1987). Coloration and darkening of methane clathrate and other ices by charged particle irradiation: Applications to the outer solar system. J. Geophys. Res., **92**, 14,933-14,947.

[17]. Grim, R.J.A. and J.M. Greenberg (1987). Photoprocessing of H_2S in interstellar grain mantles as an explanation for S_2 in comets. Astron. Astrophys., **181**, 155-168.

[18]. Khare, B.N., W.R. Thompson, B.G.J.P.T. Murray, C. Chyba and C. Sagan (1989). Solid organic residues produced by irradiation of hydrocarbon-containing H_2O and H_2O/NH_3 ices: Infrared spectroscopy and astronomical implications. Icarus **79**, 350-361.

[19]. Jenniskens, P, G.A. Baratta, A.Kouchi, M.S. de Groot, J.M. Greenberg and G. Strazzulla (1993). Carbon dust formation on interstellar grains. Astron. Astro. **273**, 583-600.

[20]. Mumma, J.J., P.R. Weissman and S.A. Stern (1993). Comets and the origin of the solar system: reading the Rosetta Stone, in *Protostars and Planets, III* (Ed. E. Levy, J.I. Lunine and M. Matthews), Univ. of Arizona Press, Tucson.

[21]. Bar-Nun, A., G. Herman and D. Laufer (1985). Trapping and release of gases by water ice and implications for icy bodies. Icarus, **63**, 317-332.

[22]. Laufer, D., E. Kochavi and A. Bar-Nun (1987). Structure and dynamics of amorphous water ice. Phys. Rev. B, **36** No. 17, 9219-9227.

[23]. Sandford, S.A., L.J. Allamandola, A.G.G.M. Tielens and G.J. Valero (1988). Laboratory studies of the infrared spectral properties of CO in astrophysical ices. Astrophysical Journal, **329**, 498-510.

[24]. Kouchi, A. (1987). Vapour pressure of amorphous H_2O ice and its astrophysical implications. Nature, **330**, 550-552.

[25]. Kouchi, A. (1990). Evaporation of H_2O-CO Ice and its Astrophysical Implications. J. Crystal Growth **99**, 1220-1226.

[26]. Kouchi, A. and T. Kuroda (1990). Evaporation of H_2O-CO_2-CH_4-CO ice and its implication for the evolution of ice grains. Proc. 24th ESLAB symp. on the formation of stars and planets, Friedrichshafen, ESA.

[27]. Kochan, H., A. Bischoff, H. Fechtig, B. Feuerbacher, E. Grun, F. Joo, J. Klinger, H. Kohl, D. Krankowsky, K. Roessler, W. Seboldt, K. Thiel, G. Schwehm and U. Weishaupt (1988). Lunar and Planetary Science **XIX**, pp. 617-618.

[28]. Hsuing, P. and K. Roessler (1990). Diffusion of volatiles in cometary analogs. LPSC **XXI**, 538-539.
[29]. Davidson, D.W., Y.P. Handa, C.I. Ratcliffe and J.S. Tse (1984). The ability of small molecules to form clathrate hydrates of structure II. Nature, **311**, 142-143.
[30]. Lebofsky, L.A. (1975). Stability of Frosts in the solar system (1975). Icarus **25**, 205-217.
[31]. New clathrate reference.
[32]. Burton and Oliver, 1935.
[33]. Dowell L.G. and A.P. Rinfret (1960). Low temperature forms of ice as studied by X-ray diffraction. Nature **188,** 1144-1148.
[34]. Narten, A.H., C.G. Venkatesh and S. Rice (1976). Diffraction pattern and structure of amorphous solid water at 10 and 77 K. J. Chem. Phys. **64(3)**, 1106-1121.
[35]. Mayer, E. and R. Pletzer (1984). Polymorphism in vapor deposited amorphous solid water. J. Chem. Phys. **80**(6), 2939-2952.
[36]. Olander, D. and S.A. Rice (1972). Proc. Natl. Acad. Sci., **69**, 98.
[37]. Sceats, M.G. and S.A. Rice (1982). In: *Water: A comprehensive Treatise*, (Ed. F. Franks), New York, Plenum, 83.
[38]. Pohorille, A., L.R. Pratt, R.A. LaViolette, M.A. Wilson and R.D. MacElroy (1987). Comparison of the structure of harmonic aqueous glasses and liquid water. J. Chem. Phys. **87**(10), 6070-6077.
[39]. Sciortino, F., A. Geiger and H.E. Stanley (1992). J. Chem. Phys., **96**, 3857.
[40]. Dubochet, J., J. Lepault, R. Freeman, J.A. Berriman and J.C. Homo (1982). Electron Microscopy of frozen water and aqueous solutions. J. Microscopy, **128**, Pt. 3, 219-237.
[41]. Heide, H.G. (1984). Observations on ice layers. Ultramicroscopy. **14**, 271-278.
[42]. Heide, H.G. and E. Zeitler (1985). The physical behavior of solid water at low temperatures and the embedding of electron microscopical specimens. Ultramicrosc. **16**, 151-160.
[43]. Sivakumar, T.C., D. Schuh, M.G Sceats and S.A. Rice (1977). Chem. Phys. Lett., **48**, 212.
[44]. Sivakumar, T.C., S.A. Rice and M.C. Sceats (1978). J. Chem. Phys., **69**, 3468.
[45]. Jenniskens, P. and D.F. Blake (1994). "Structural transitions in amorphous water ice and astrophysical implications." Science, **265**:753-756.
[46]. Mishima, O., L.D. Calvert and E. Whalley (1984). Nature, **310**, 393.
[47]. Mishima, O., L.D. Calvert and E. Whalley (1985). Nature, **314**, 393.
[48]. Handa, Y.P., O. Mishima and E. Whalley (1986). J. Chem. Phys. **84**, 2766.
[49]. Bzid et al, 1987.
[50]. Tse, J.S. and M.L. Klein (1987). Phys. Rev. Lett. **58**, 1672.
[51]. Hemley, Chen and Mao, 1989.
[52]. Bosio, L., G.P Johari and J. Teixera (1986). Phys. Rev. Lett. **56**, 460. Burton, E.F. and W.F. Oliver (1935). Proc. Roy Soc. (London), **A153**, 166. Bizid, A.,

L. Bosio, A. Defrain, and M. Oumezzine (1987). "Structure of high-density amorphous water. I. X-ray diffraction study." J. Chem. Phys. **874:**2225-2230.

[53]. Tse, J.S. (1992). J. Chem. Phys. **96**, 5482.

[54]. McMullen and Los (1965). Vitreous ice: irreversible transformations during warm-up. Nature **206** 806-810.

[55]. Ghormley, J.A. (1968). J. Chem. Phys. **48**, 503.

[56]. Sugisaki, M., H. Suga and S. Seki (1968). Bull. Chem. Soc. Japan **41**, 2591.

[57]. Hallbrucker, A., E. Mayer and G.P. Johari (1989). Glass Transition in Pressure-Amorphosed Hexagonal Ice. A Comparison with Amorphous forms made from the Vapor and Liquid. J. Phys. Chem. **93**, 7751-7752.

[58]. Blake, D.F. and G. Palmer (1991). Analysis of cometary and interstellar ice analogs in the electron microscope. Microbeam Analysis — 1991, 293-298.

[59]. Mayer, E. and R. Pletzer (1986). Nature **319**, 298.

[60]. Schmitt, B., S. Espinasse, R.J.A. Grim, J.M. Greenberg, J. Klinger (1989). "Laboratory studies of cometary ice analogues." In: Proc. of the International Workshop on Physics and Mechanics of Cometary Materials, J. Hunt, T.D. Guyenne, eds., (European Space Agency, Paris), vol. ESA SP-302, pp. 65-69.

[61]. Schutte, W.A. (1988). Thesis, University of Leiden, Leiden, Netherlands.

[62]. van IJzendoorn, L.J. (1985). Thesis, University of Leiden, Leiden, Netherlands.

[63]. Jenniskens, P., D.F. Blake, M. Wilson, and A. Pohorille (1995). "High density amorphous ice, the frost on interstellar grains." Astrophysical Journal **455**:389-401.

[64]. Fujime, S. (1966). "Electron Diffraction at Low Temperature II. Radial Distribution Analysis of Metastable Structure of Metal Films Prepared by Low Temperature Condensation." Japanese Journal of Applied Physics **59:**764-777.

[65]. Moine, P., A.R. Pelton and R. Sinclair (1988). "Structural Determination of Small Amorphous Volumes by Electron Diffraction." Journal of Non-Crystalline Solids, **101:**213-222.

[66]. Wilson, M.A., A. Pohorille, P. Jeniskens and David F. Blake (1995). "Probing the structure of cometary ice." Origins of Life and Evolution of the Biosphere **25**:3-19

[67]. Yannas, I. (1968). "Vitrification Temperature of Water." Science **160:**298-299.

[68]. Rasmussen, D. H. and A. MacKenzie (1971). "The Glass Transition in Amorphous Water. Application of the Meausurements to Problems Arising in Cryobiology." J. Phys. Chem. **75**967-973.

[69]. Blake, D.F., L. Allamandola, S. Sandford, D. Hudgins and F. Freund (1991b). Clathrate Hydrate Formation in Amorphous Cometary Ice Analogs in Vacuo. *Science*, **254**, 548-551

[70]. Jenniskens, P., S. F. Banham, D.F. Blake and M.R.S. McCoustra (1996). "Liquid Water In the Domain of Cubic Crystalline Ice, Ic." J. Chem. Phys.,